

Surface and 3D Quantum Hall Effects from Engineering of Exceptional Points in Nodal-Line Semimetals

Rafael A. Molina and José González

Instituto de Estructura de la Materia—CSIC, Serrano 123, E-28006 Madrid, Spain

 (Received 16 October 2017; revised manuscript received 25 January 2018; published 5 April 2018)

We show that, under a strong magnetic field, a 3D nodal-line semimetal is driven into a topological insulating phase in which the electronic transport takes place at the surface of the material. When the magnetic field is perpendicular to the nodal ring, the surface states of the semimetal are transmuted into Landau states which correspond to exceptional points, i.e., branch points in the spectrum of a non-Hermitian Hamiltonian which arise upon the extension to complex values of the momentum. The complex structure of the spectrum then allows us to express the number of zero-energy flat bands in terms of a new topological invariant counting the number of exceptional points. When the magnetic field is parallel to the nodal ring, we find that the bulk states are built from the pairing of surfacelike evanescent waves, giving rise to a 3D quantum Hall effect with a flat level of Landau states residing in parallel 2D slices of the 3D material. The Hall conductance is quantized in either case in units of e^2/h , leading in the 3D Hall effect to a number of channels growing linearly with the section of the surface and opening the possibility to observe a macroscopic chiral current at the surface of the material.

DOI: [10.1103/PhysRevLett.120.146601](https://doi.org/10.1103/PhysRevLett.120.146601)

Introduction.—Currently, there is a huge amount of interest in the new family of 3D topological semimetals, which include Dirac and Weyl semimetals with isolated Dirac or Weyl nodes in the band structure [1–6], and the nodal-line semimetals (NLSMs) with a continuous line of nodes in the Brillouin zone [7,8]. There are already several experimentally established examples of topological NLSMs, including PbTaSe_2 [9], PtSn_4 [10], and ZrSiS [11]. Apart from the theoretical interest, as their low-energy excitations behave as relativistic fermions, they exhibit very remarkable features, like the presence of a 2D manifold of surface states forming nearly flat or very narrow bands, with the potential for very strong correlations [12].

Another relevant instance leading to a large degeneracy of electronic states arises in low-temperature 2D samples in the presence of a strong magnetic field, where the Hall conductivity can be quantized as first discovered by von Klitzing *et al.* [13]. The explanation of this phenomenon is the paradigmatic example of the application of topological concepts in condensed matter physics. The integer values dictating the quantization of the Hall conductivity can be written in terms of topological invariants known as Chern numbers, closely related to Berry phases [14].

As long as the 2D quantum Hall effect is supported by boundary states, it turns out to be quite interesting to ask about the new physical effects which may arise from the plethora of surface states of a 3D NLSM in a strong magnetic field. In this setting, it becomes relevant to investigate whether the manifold of surface states may build a quantized 3D Hall effect, and the kind of boundary states which may support the electronic transport in the 3D material.

Several studies have investigated the effect of a strong magnetic field in 3D semimetals [15,16]. It has been proposed, for instance, that closed orbits can be formed in the bulk by connecting the Fermi arcs at opposite surfaces of 3D Weyl semimetals, allowing for a quantum Hall effect [17,18]. In the case of the NLSMs, the possibility has been shown of having a zero-energy level and Landau bands following a pattern similar to that from Dirac fermions [19].

In this Letter, we unveil the potential of the 3D NLSMs to support a phenomenon which is the analogue of the 2D quantum Hall effect but promoted to a higher spatial dimension. We are going to see that, when the magnetic field is perpendicular to the nodal ring, the evanescent states of the NLSM remain stabilized in a zero-energy level with huge 2D degeneracy arising from the collapse down to zero energy of a large number of 2D-like Landau levels. On the other hand, a magnetic field parallel to the nodal ring has the effect of pairing the evanescent waves *inside* the bulk of the NLSM, leading to states that reside in parallel 2D slices of the 3D material. This constitutes then a perfect version of a 3D quantum Hall effect [20], of which very few examples are known [21–25]. In either case, the low-energy bulk states in 3D slab geometries turn out to be localized, while only the surface states contribute to the electronic transport (as shown schematically in Fig. 1).

We will see that the topological protection of the evanescent states in a strong magnetic field lies in their connection to exceptional points, i.e., branch points which arise upon extension of the spectrum to complex values of the momentum [26,27]. The properties of the exceptional points have been recently applied to describe several

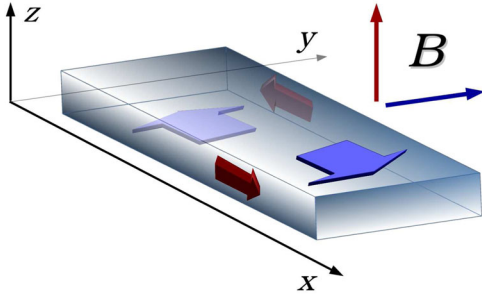


FIG. 1. Schematic plot of the surface electronic currents in a slab of 3D NLSM for two orthogonal directions of the magnetic field.

unconventional features in electron systems [28–30]. Exceptional points have been also found in the study of non-Hermitian Hamiltonians [31] and the experimental observation of photonic crystals [32]. In the present context, we will see that the exceptional points can be applied to build a new topological index addressing the stability and quantization of the Hall effect in 3D NLSMs.

Surface Hall effect.—Our starting point is a continuum model of NLSM, whose suitability is well documented from the description of the compounds of the CaP₃ family [33]. In units in which $\hbar = 1$ [34], the Hamiltonian is given by

$$H_{\text{NL}} = (m_0 + m_1 \nabla^2) \sigma_z - iv \partial_z \sigma_x, \quad (1)$$

where σ_i ($i = x, y, z$) stand for the Pauli matrices. In terms of the 3D momentum \mathbf{k} , the model displays two bands with energy

$$\varepsilon = \pm \sqrt{(m_0 - m_1 \mathbf{k}^2)^2 + v^2 k_z^2}. \quad (2)$$

We find a line of nodes where the two bands meet in the plane $k_z = 0$, corresponding to the circular set $k_x^2 + k_y^2 = m_0/m_1$. A remarkable feature is that the projection of the nodal ring onto a given surface leads to a so-called drumhead, filled by surface states forming in general nearly flat or very narrow bands.

In the presence of a magnetic field in the z direction (perpendicular to the plane of the nodal line), the vector potential can be written as $\mathbf{A} = (-By, 0, 0)$. Setting units in which $e = 1$ and $c = 1$, the Hamiltonian of the NLSM becomes

$$H_{\perp} = (m_0 + m_1 [-(i\partial_x - By)^2 + \partial_y^2 + \partial_z^2]) \sigma_z - iv \partial_z \sigma_x. \quad (3)$$

The eigenstates in the bulk of the semimetal are given in terms of the eigenfunctions of a harmonic oscillator centered at $y = k_x/B$, with energy eigenvalues

$$\varepsilon_n = \pm \sqrt{[m_0 - m_1 k_x^2 - 2m_1 B(n + 1/2)]^2 + v^2 k_z^2}, \quad (4)$$

where $n \geq 0$ is the Landau level index.

On the other hand, eigenstates decaying from a 2D boundary of the semimetal (at $z = 0$) take the form

$$\Psi \sim e^{iwz} \chi(x, y) \hat{\eta}, \quad (5)$$

with $w = k_z + i\alpha$. Taking $\hat{\eta}$ such that $\sigma_y \hat{\eta} = \pm \hat{\eta}$, a pair of zero-energy eigenstates can be found for each sign of the pseudospin σ_y . In the model with $4m_0 m_1 < v^2$, for instance, the zero-energy evanescent states are given by

$$w = \pm i \frac{v \pm \sqrt{v^2 - 4m_1 [m_0 - m_1 2B(n + 1/2)]}}{2m_1} \quad (6)$$

where the sign in front the right-hand side of Eq. (6) matches the sign of the pseudospin σ_y .

This construction reveals that, in the presence of a magnetic field perpendicular to the nodal ring, the drumhead surface states are converted into Landau states decaying from the surface of the NLSM. In general, this transmutation leads to the collapse of a great number of Landau levels down to zero energy. This degeneracy applies to Landau levels with order n such that $m_0 - 2m_1 B(n + 1/2) > 0$, up to a maximum value beyond which the condition (6) inverts the sign of one of the momenta. The band structure for a slab of width $W = 40$ nm (in the z direction) in a magnetic field with $B = 30$ T is represented in Fig. 2, which illustrates the huge degeneracy of Landau states in the zero-energy level.

The zero modes of (3) indeed have a deep meaning. The Hamiltonian has particle-hole symmetry, realized as $\sigma_y H_{\perp} \sigma_y = -H_{\perp}$, so that zero-energy eigenvalues correspond to points in the complex plane (k_z, α) where two eigenstates Ψ and $\sigma_y \Psi$ coalesce. This is the distinctive feature of an exceptional point—that is, a branch point singularity where two different branches of the complex

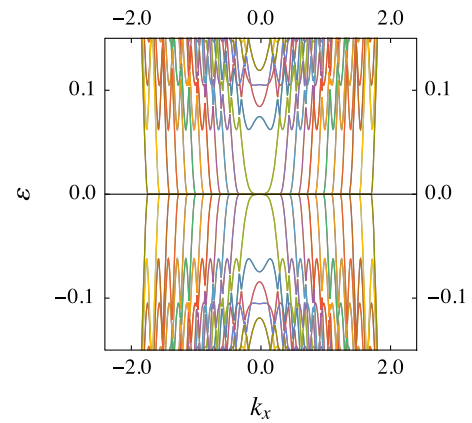


FIG. 2. Band structure for a slab of NLSM of width $W = 40$ nm (lateral dimension $\Delta y = 40$ nm), for parameters $m_0 = 1.2$ eV, $m_1 = 1.0$ eV nm², $v = 0.5$ eV nm, and magnetic field (perpendicular to the nodal ring) $B = 30$ T. The energy is measured in electron-volts and the momentum in inverse nanometers.

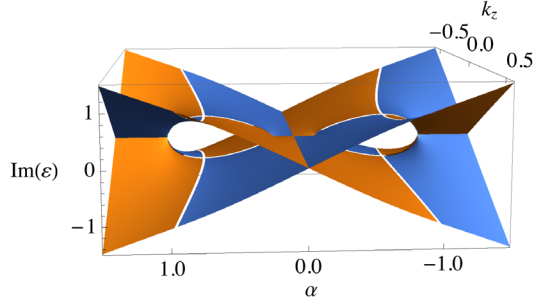


FIG. 3. Spectrum of a NLSM (with $m_0 = 0.2$ eV, $m_1 = 0.8$ eV nm², $v = 1.0$ eV nm, and magnetic field perpendicular to the nodal ring $B = 30$ T) for complex momenta $k_z + i\alpha$ (k_z being perpendicular to the nodal ring) showing two branch cuts connecting pairs of exceptional points along the α axis. The energy is measured in electron-volts and the momentum in inverse nanometers.

spectrum meet. This can be seen in Fig. 3, which shows the Riemann sheet of the spectrum of a NLSM for $n = 0$.

Such exceptional points are at the origin of the topological protection of the surface Landau states under very general perturbations preserving the particle-hole symmetry. In the case of a periodic perturbation $U(x, y)$, the eigenvalue problem can be written as

$$[H_{\perp} + U(x, y)\sigma_z]\chi(x, y)\eta(z) = \epsilon\chi(x, y)\eta(z). \quad (7)$$

It can be shown that the quantization of the Hall conductivity σ_{xy} is enforced by the Chern number corresponding to the connection $A_j = i \int dx dy \chi^*(\partial/\partial k_j)\chi$ [35]. Nevertheless, not all the 2D Landau levels give rise to surface Landau states, as these require the superposition of zero-energy solutions $\eta(z) \sim e^{i\nu z}\hat{\eta}$ with equal $\hat{\eta}$ and the same sign of $\text{Im}(w)$. This amounts to counting pairs of exceptional points with the same pseudospin in the upper half of the complex plane, which is accomplished by the index

$$\nu = \frac{1}{2\pi i} \sum_n' \oint_C dw \frac{1}{\epsilon_n(w)} \frac{d}{dw} \epsilon_n(w), \quad (8)$$

where the contour C is stretched in the upper half-plane to cover all possible singularities, and the prime means that the sum is carried over the subbands n for which the expectation value of the pseudospin $\langle\sigma_y\rangle$ keeps the same sign in all the region inside the contour [35]. The index ν acts then as a topological invariant for the surface Hall effect, as long as the analyticity properties in the complex plane dictate its insensitivity to regular perturbations of the contour or the integrand in Eq. (8) [36].

It is worthwhile to note that single evanescent solutions like those given by Eqs. (5) and (6) (valid in the limit of infinite depth W along the z direction) cannot carry a current along the x direction, as the current operator is given by $j_x = -2m_1(k_x - By)\sigma_z$ while the evanescent

waves are eigenstates of σ_y . However, this does not hold in the case of a slab with finite width W , as the two evanescent waves attached to opposite faces of the slab start to hybridize when approaching the boundaries of the lateral dimension Δy , leading to a chiral current along the vertical surface, as shown in Fig. 1. This explains the dispersion of the bands from the zero-energy Landau level in Fig. 2, which implies a nonvanishing current as $\langle j_x \rangle = \partial\epsilon/\partial k_x$. The N -fold degeneracy of the zero-energy level leads then to a transverse Hall conductivity $\sigma_{xy} = N(e^2/h)$, where the number of channels may be as large as $N \sim 30$ for $B = 10$ T and parameters $m_0 \sim 1$ eV, $m_1 \sim 1.0$ eV nm².

3D Hall effect.—We consider now the case in which the magnetic field is parallel to the plane of the nodal line, taking for definiteness a constant field pointing in the y direction. The vector potential can be chosen as $\mathbf{A} = (Bz, 0, 0)$, and the Hamiltonian reads in that gauge

$$H_{\parallel} = (m_0 + m_1[-(-i\partial_x + Bz)^2 + \partial_y^2 + \partial_z^2])\sigma_z - iv\partial_z\sigma_x. \quad (9)$$

In this case, the most interesting effects manifest again in a slab with finite width W in the z direction. In this geometry, there is a highly degenerate level at virtually zero energy which arises from the collapse of a large number of flat bands corresponding to different values of the momentum k_y . This is represented in Fig. 4, where we can see the band structure for a slab of width $W = 60$ nm, under a magnetic field with $B = 30$ T.

Quite remarkably, the states in the highly degenerate zero-energy level are localized at parallel 2D slices within the bulk of the slab. A typical shape of wave function along the z direction for a state in the zero Landau level can be

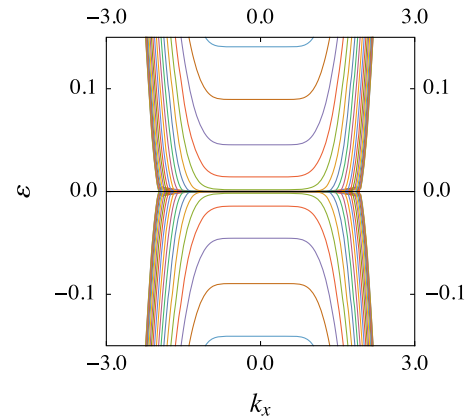


FIG. 4. Band structure for a slab of NLSM of width $W = 60$ nm (lateral dimension $\Delta y = 60$ nm), for parameters $m_0 = 0.5$ eV, $m_1 = 0.5$ eV nm², $v = 0.5$ eV nm, and magnetic field (parallel to the nodal ring) $B = 30$ T. The units are the same as in Fig. 2.

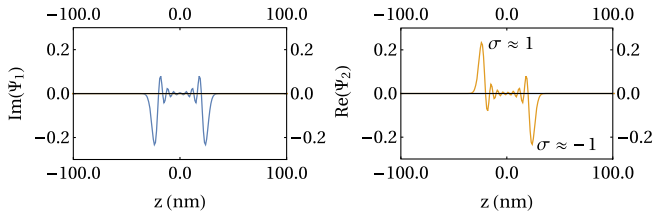


FIG. 5. Plot of the wave function along the direction perpendicular to the nodal ring (zoom view) showing the imaginary part of the first component [as $\text{Re}(\Psi_1) = 0$], and the real part of the second component [as $\text{Im}(\Psi_2) = 0$] of a state with $k_x = k_y = 0$ in the zero Landau level of a NLSM with $m_0 = 2.0$ eV, $m_1 = 1.5$ eV nm², $v = 0.5$ eV nm, and magnetic field (parallel to the nodal ring) $B = 30$ T. The figure also shows the pseudospin $\sigma = \langle \sigma_y \rangle$ of the two evanescent waves making up the state.

seen in Fig. 5. The localization of the state in the bulk can be moved by varying the momentum k_x , which shifts the center of the slice z_0 within the slab.

The unconventional character of the quasi-2D states in the bulk is displayed by the fact that they arise from the superposition of two waves, both evanescent along z but with opposite orientations. The possibility of having those waves can be realized from inspection of the eigenvalue problem (for $k_x = k_y = 0$),

$$[m_0 + m_1(\partial_z^2 - B^2 z^2)]\sigma_z \Psi - iv\partial_z \sigma_x \Psi = \epsilon \Psi. \quad (10)$$

Equation (10) looks like a Dirac equation for massive fermions in which the magnetic field provides a confining potential. Thus, the potential well gives rise to two domain walls (turning points) along the z direction which are able to pin the evanescent waves, leading to localized eigenstates within the gap opened by the mass in the Dirac spectrum.

We can make contact at this point with the physics of the evanescent waves and exceptional points of the previous section. The two evanescent waves that now make up each quasi-2D localized state have, to a good approximation, well-defined opposite values of the pseudospin σ_y . This is evidenced in Fig. 5 by the change of sign in $\text{Re}(\Psi_2)$ when passing from one evanescent wave to the other. Anyhow, there is always some interaction between the two evanescent waves [37], which accounts for the fact that they may carry small (and opposite) contributions to the current density $j_x = -2m_1(k_x + Bz)\sigma_z$. These cancel out when integrating along z , except when the slice of the quasi-2D state approaches one of the faces of the slab. Then the evanescent waves get distorted, so that one of the contributions to j_x starts to prevail. This explains the fact that the electronic current is confined to the surface of the NLSM, taking opposite orientations at opposite faces of the slab.

The huge degeneracy of the zero Landau level affords a quantization of the 3D Hall conductivity. This can be

shown by observing that the current density j_x is equal to the derivative $\partial H_{\parallel} / \partial k_x$. Thus, the current of each state across a section of the slab (for a finite lateral dimension Δy) is given in terms of the dispersion $\epsilon(k_x)$ by

$$\frac{1}{W} \frac{1}{\Delta y} \int dy dz \Psi^\dagger j_x \Psi = \frac{\partial \epsilon}{\partial k_x}. \quad (11)$$

Considering the situation in which the Fermi level is right above the zero Landau level, we obtain the intensity I_x along the x direction by integrating over all the filled states in the bands dispersing from zero energy. We get (reinstating at this point \hbar in the equations)

$$I_x = \frac{e}{\hbar} \int_{\text{filled states}} \frac{dk_x}{2\pi} \frac{\partial \epsilon}{\partial k_x}. \quad (12)$$

The integral in (12) is nothing but the difference between the respective chemical potentials ϵ_+ , ϵ_- at the two opposite faces of the slab times the degeneracy N of the zero Landau level. Therefore, we have $I_x = N(e/h)(\epsilon_+ - \epsilon_-)$ and the Hall conductance $G = N(e^2/h)$.

It is important to realize that the zero-mode degeneracy N (observed, for instance, in Fig. 4) scales with the lateral dimension Δy . The different flat bands collapsed down to zero energy correspond to different quantized values of the momentum k_y . We add a new degenerate band for each wave number of the original drumhead that can be accommodated in the finite lateral dimension, up to a maximum momentum \tilde{K}_y reaching the limit of the nodal ring. The number of channels N is indeed given by $\tilde{K}_y \Delta y / 2\pi$. Therefore, according to the orientation in Fig. 1, the 3D Hall conductivity can be written as

$$\sigma_{zx} = \frac{e^2}{h} e_{zxy} \frac{\tilde{K}_y}{2\pi}. \quad (13)$$

This result is consistent with the formula obtained by Halperin for the Hall conductivity in 3D gapped systems [20]. As in Ref. [20], $2\pi/\tilde{K}_y$ has the meaning of the wavelength of an oscillation, which in the present context corresponds to the minimum wavelength of the quantized waves fitting in the lateral dimension Δy .

Conclusions.—We have shown that, under a strong magnetic field, a 3D NLSM enters a topological insulating phase in which the low-energy states in the bulk do not contribute to the conductivity, and all the electronic transport takes place at the surface of the material.

A distinctive feature of the surface and 3D Hall effects in NLSMs is that they are based on the existence of evanescent states with a well-defined pseudospin. The pseudospin operator realizes the particle-hole transformation in the electron system, which explains that such evanescent states correspond to exceptional points—that is, branch points

where two states with opposite energy coalesce in the spectrum of the NLSM.

In general, we may expect that a surface Hall effect may survive when the NLSM is under perturbations with a strength smaller than the gap between the zero-energy Landau level and the next higher bands. We have seen, however, that when the perturbations preserve the particle-hole symmetry, the complex structure tied to the exceptional points lends a much larger stability to the zero-energy flat bands in the spectrum [35]. In these conditions, the Hall conductivity can be expressed in terms of the integral of a suitable Berry connection, in the same fashion as in the 2D Hall effect. As a counterpart, we have also shown that the complex structure of the spectrum (for complex values of the momentum) allows us to express the number of zero-energy flat bands in terms of a different topological invariant, counting essentially the number of exceptional points and ensuring its topological character from the impossibility of removing such branch points by smooth perturbations of the spectrum.

We are grateful to F. Barbero for fruitful discussions. We acknowledge financial support through Spanish MINECO/FEDER Grants No. FIS2014-57432-P, No. FIS2015-63770-P, and No. FIS2017-82260-P, and through CAM research consortium Grant No. QUITEMAD+ S2013/ICE2801.

-
- [1] X. Wan, A. M. Turner, A. Vishwanath, and S. Y. Savrasov, Topological semimetal and Fermi-arc surface states in the electronic structure of pyrochlore iridates, *Phys. Rev. B* **83**, 205101 (2011).
- [2] A. A. Burkov and L. Balents, Weyl Semimetal in a Topological Insulator Multilayer, *Phys. Rev. Lett.* **107**, 127205 (2011).
- [3] Z. K. Liu, B. Zhou, Y. Zhang, Z. J. Wang, H. M. Weng, D. Prabhakaran, S.-K. Mo, Z. X. Shen, Z. Fang, X. Dai, Z. Hussain, and Y. L. Chen, Discovery of a three-dimensional topological Dirac semimetal, Na_3Bi , *Science* **343**, 864 (2014).
- [4] M. Neupane, S.-Y. Xu, R. Sankar, N. Alidoust, G. Bian, C. Liu, I. Belopolski, T.-R. Chang, H.-T. Jeng, H. Lin, A. Bansil, F. Chou, and M. Z. Hasan, Observation of a three-dimensional topological Dirac semimetal phase in high-mobility Cd_3As_2 , *Nat. Commun.* **5**, 3786 (2014).
- [5] S. Borisenko, Q. Gibson, D. Evtushinsky, V. Zabolotnyy, B. Büchner, and R. J. Cava, Experimental Realization of a Three-Dimensional Dirac Semimetal, *Phys. Rev. Lett.* **113**, 027603 (2014).
- [6] S.-Y. Xu, I. Belopolski, N. Alidoust, M. Neupane, G. Bian, C. Zhang, R. Sankar, G. Chang, Z. Yuan, C.-C. Lee, S.-M. Huang, H. Zheng, J. Ma, D. S. Sanchez, B. Wang, A. Bansil, F. Chou, P. P. Shibayev, H. Lin, S. Jia, and M. Z. Hasan, Discovery of a Weyl fermion semimetal and topological Fermi arcs, *Science* **349**, 613 (2015).
- [7] A. A. Burkov, Topological semimetals, *Nat. Mater.* **15**, 1145 (2016).
- [8] C. Fang, H. Weng, X. Dai, and Z. Fang, Topological nodal line semimetals, *Chin. Phys. B* **25**, 117106 (2016).
- [9] G. Bian *et al.*, Topological nodal-line fermions in spin-orbit metal PbTaSe_2 , *Nat. Commun.* **7**, 10556 (2016).
- [10] Y. Wu, L.-L. Wang, E. Mun, D. D. Johnson, D. Mou, L. Huang, Y. Lee, S. L. Bud'ko, P. C. Canfield, and A. Kaminski, Dirac node arcs in PtSn_4 , *Nat. Phys.* **12**, 667 (2016).
- [11] L. M. Schoop, M. N. Ali, C. Straer, V. Duppel, S. S. P. Parkin, B. V. Lotsch, and C. R. Ast, Dirac cone protected by non-symmorphic symmetry and 3D Dirac line node in ZrSiS , *Nat. Commun.* **7**, 11696 (2015).
- [12] S. Jia, S.-Y. Xu, and M. Z. Hasan, Weyl semimetals, Fermi arcs and chiral anomaly, *Nat. Mater.* **15**, 1140 (2016).
- [13] K. von Klitzing, G. Dorda, and M. Pepper, New Method for High-Accuracy Determination of the Fine-Structure Constant Based on Quantized Hall Resistance, *Phys. Rev. Lett.* **45**, 494 (1980).
- [14] D. J. Thouless, M. Kohmoto, M. P. Nightingale, and M. den Nijs, Quantized Hall Conductance in a Two-Dimensional Periodic Potential, *Phys. Rev. Lett.* **49**, 405 (1982).
- [15] K.-Y. Yang, Y.-M. Lu, and Y. Ran, Quantum Hall effects in a Weyl semimetal: Possible application in pyrochlore iridates, *Phys. Rev. B* **84**, 075129 (2011).
- [16] J. Cao, S. Liang, C. Zhang, Y. Liu, J. Huang, Z. Jin, Z.-G. Chen, Z. Wang, Q. Wang, J. Zhao, S. Li, X. Dai, J. Zou, Z. Xia, L. Li, and F. Xiu, Landau level splitting in Cd_3As_2 under high magnetic fields, *Nat. Commun.* **6**, 7779 (2015).
- [17] A. C. Potter, I. Kimchi, and A. Vishwanath, Quantum oscillations from surface Fermi arcs in Weyl and Dirac semimetals, *Nat. Commun.* **5**, 5161 (2014).
- [18] C. M. Wang, H.-P. Sun, H.-Z. Lu, and X. C. Xie, 3D Quantum Hall Effect of Fermi Arcs in Topological Semimetals, *Phys. Rev. Lett.* **119**, 136806 (2017).
- [19] J.-W. Rhim and Y. B. Kim, Landau level quantization and almost flat modes in three dimensional semimetals with nodal ring spectra, *Phys. Rev. B* **92**, 045126 (2015).
- [20] B. I. Halperin, Possible states for a three-dimensional electron gas in a strong magnetic field, *Jpn. J. Appl. Phys.* **26**, 1913 (1987).
- [21] M. Koshino, H. Aoki, and B. I. Halperin, Wrapping current versus bulk integer quantum Hall effect in three dimensions, *Phys. Rev. B* **66**, 081301(R) (2002).
- [22] V. P. Nair and S. Randjbar-Daemi, Quantum Hall effect on S^3 , edge states and fuzzy S^3/\mathbb{Z}_2 , *Nucl. Phys.* **B679**, 447 (2004).
- [23] B. A. Bernevig, T. L. Hughes, S. Raghu, and D. P. Arovas, Theory of the Three-Dimensional Quantum Hall Effect in Graphite, *Phys. Rev. Lett.* **99**, 146804 (2007).
- [24] K. Hasebe, Chiral topological insulator on Nambu 3-algebraic geometry, *Nucl. Phys.* **B886**, 681 (2014).
- [25] K. Mullen, B. Uchoa, and D. T. Glatzhofer, Line of Dirac Nodes in Hyperhoneycomb Lattices, *Phys. Rev. Lett.* **115**, 026403 (2015).
- [26] M. V. Berry, Physics of non-Hermitian degeneracies, *Czech. J. Phys.* **54**, 1039 (2004).
- [27] W. D. Heiss, The physics of exceptional points, *J. Phys. A* **45**, 444016 (2012).
- [28] P. San-José, J. Cayao, E. Prada, and R. Aguado, Majorana bound states from exceptional points in non-topological superconductors, *Sci. Rep.* **6**, 21427 (2016).

- [29] J. González and R. A. Molina, Macroscopic Degeneracy of Zero-Mode Rotating Surface States in 3D Dirac and Weyl Semimetals under Radiation, *Phys. Rev. Lett.* **116**, 156803 (2016).
- [30] J. González and R. A. Molina, Topological protection from exceptional points in Weyl and nodal-line semimetals, *Phys. Rev. B* **96**, 045437 (2017).
- [31] H. Shen, B. Zhen, and L. Fu, Topological Band Theory for Non-Hermitian Hamiltonians, [arXiv:1706.07435](https://arxiv.org/abs/1706.07435).
- [32] H. Zhou, C. Peng, Y. Yoon, C. W. Hsu, K. A. Nelson, L. Fu, J. D. Joannopoulos, M. Soljacic, and B. Zhen, Observation of bulk Fermi arc and polarization half charge from paired exceptional points, [arXiv:1709.03044](https://arxiv.org/abs/1709.03044).
- [33] Z. Xu, R. Yu, Z. Fang, X. Dai, and H. Weng, Topological nodal line semimetals in CaP_3 family of materials, *Phys. Rev. B* **95**, 045136 (2017).
- [34] We recover fully dimensional units when discussing conductance in terms of the conductance quantum e^2/h .
- [35] See Supplemental Material at <http://link.aps.org/supplemental/10.1103/PhysRevLett.120.146601> for the topological invariance and the quantization of the Hall conductivity in the surface Hall effect.
- [36] The expression of the index ν bears also similarities with that of the winding number derived for non-Hermitian $\text{SU}(1,1)$ Hamiltonians by K. Esaki, M. Sato, K. Hasebe, and M. Kohmoto, *Phys. Rev. B* **84**, 205128 (2011).
- [37] Increasing the field strength B brings closer the evanescent waves, raising their energy gradually until it gets a sensible nonvanishing value. Thus, for very large magnetic fields (with $B \gtrsim 60$ T), a gap opens up in the zero Landau level and the massive degeneracy is lost.